

Crystal structures of the catalytic domain of human protein kinase associated with apoptosis and tumor suppression

Valentina Tereshko^{1,2,3}, Marianna Teplova^{1,2,3}, Joseph Brunzelle⁴, D. Martin Watterson⁴ and Martin Egli¹

We have determined X-ray crystal structures with up to 1.5 Å resolution of the catalytic domain of death-associated protein kinase (DAPK), the first described member of a novel family of pro-apoptotic and tumor-suppressive serine/threonine kinases. The geometry of the active site was studied in the apo form, in a complex with nonhydrolyzable AMPPnP and in a ternary complex consisting of kinase, AMPPnP and either Mg²⁺ or Mn²⁺. The structures revealed a previously undescribed water-mediated stabilization of the interaction between the lysine that is conserved in protein kinases and the β- and γ-phosphates of ATP, as well as conformational changes at the active site upon ion binding. Comparison between these structures and nucleotide triphosphate complexes of several other kinases disclosed a number of unique features of the DAPK catalytic domain, among which is a highly ordered basic loop in the N-terminal domain that may participate in enzyme regulation.

Programmed cell death (apoptosis) is key to normal development, and alterations of its control have been implicated in human disease, including the loss of tumor suppression linked to cancer progression^{1–5}. Multiple intracellular protein phosphorylation pathways have been implicated in apoptosis induction and control (reviewed in refs 6,7). Recently, a calmodulin (CaM)-regulated serine/threonine protein kinase termed death-associated protein kinase (DAPK) has been identified as a positive mediator of apoptosis and a regulator of tumor suppression^{8,9}. DAPK features a multidomain structure (Fig. 1), comprising eight ankyrin repeats (a 33-amino acid repeat that has been implicated in mediating protein–protein interactions), P-loops (a mononucleotide-binding sequence motif), a cytoskeleton-binding region, a death-domain and a catalytic (kinase) domain^{10–13} that has high sequence similarity to vertebrate myosin light chain kinase (MLCK). Like MLCK, DAPK does not require phosphorylation for activation.

DAPK was the first described member of a family of pro-apoptotic serine/threonine kinases, which includes at least four other kinases with significant homology in their catalytic domain to DAPK^{14,15}. ZIP(Dlk)-kinase, a serine/threonine kinase with a C-terminal leucine zipper domain, and DAPK-related protein-1 (DRP-1) are both closely related to DAPK, and their catalytic domains show ~80% identity with that of DAPK^{15–17}. By comparison, DAPK-related apoptosis-inducing

protein kinases DRAK1 and DRAK2 display ~50% identity to DAPK in their catalytic domain¹⁸. ZIP-kinase and DRAK1 and DRAK2 are nuclear proteins that do not require Ca²⁺ and calmodulin for activation. Conversely, DRP-1 is a cytoplasmic kinase whose CaM regulatory domain is similar to that of DAPK^{15,19}.

Although the kinase region of DAPK and related protein kinases has been implicated in their cellular functions^{13–19}, little is known about the properties of this essential catalytic domain. For example, endogenous protein kinase substrates for DAPK have yet to be determined, and efficient peptide substrates that allow the characterization of the enzyme activity of DAPK have been described only recently²⁰. As part of an effort to better define potentially unique properties of the catalytic domain of DAPK and gain insight into the structural features of this new family of protein kinases linked to apoptosis and tumor suppression, we have determined the three-dimensional structure of the catalytic domain of DAPK in two crystal forms. Comparison of the structures of the apo form, the complex with an ATP analog, and those of other CaM-dependent serine/threonine kinases and cyclic AMP-dependent kinase reveals several unusual properties of the DAPK catalytic domain. In addition to filling the gap in knowledge about the structural properties DAPK and related enzymes, the structure can provide a starting point for structure-assisted discovery of substrates and inhibitors.

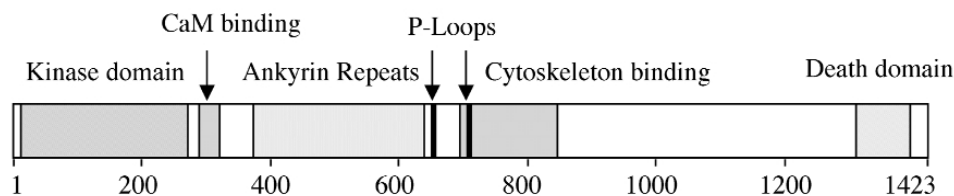


Fig. 1 Domain organization of DAPK (numbers refer to amino acids).

¹Department of Biological Sciences, Vanderbilt University, Nashville, Tennessee 37235, USA. ²These authors contributed equally to this work. ³Current address: Cellular Biochemistry and Biophysics Program, Memorial Sloan-Kettering Cancer Center, New York, New York 10021, USA. ⁴Department of Molecular Pharmacology and Biological Chemistry, Northwestern University Medical School, Chicago, Illinois 60611, USA.

Correspondence should be addressed to M.E. *email: martin.egli@vanderbilt.edu*

articles

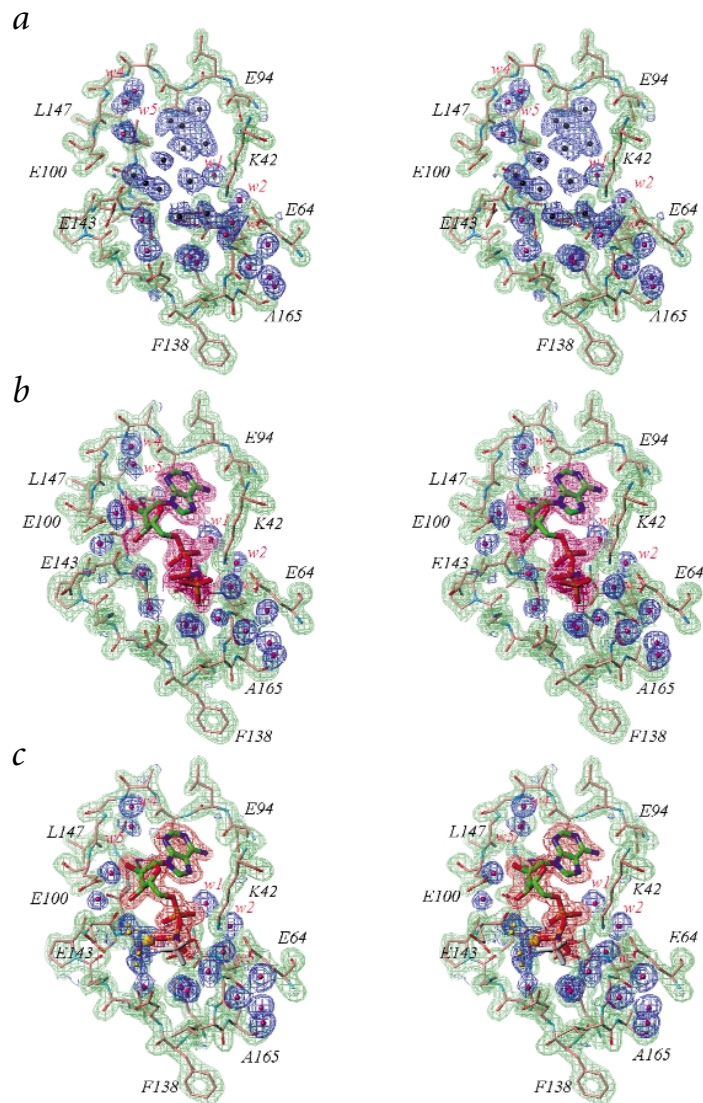


Fig. 2 Final electron density and nucleotide binding site geometry. Stereo diagrams illustrating the quality of the electron density in the orthorhombic structures of the DAPK ATP binding region and solvent rearrangements following binding of the triphosphate substrate analog. **a**, DAPK Apo-I form. **b**, Binary complex with AMPPnP. **c** Ternary complex with AMPPnP and Mn^{2+} . Omit electron density at the 2.5σ level (difference map) is drawn in green (protein), blue (active site water molecules) and red (AMPPnP). The protein region displayed comprises residues 94-ELVAGGE-100, 137-HFDLKPENIML-147 and 161-DFGLA-165 in the helix-rich lobe and Lys 42 and Glu 64 (conserved residues are underlined) from the mostly β -stranded lobe. Protein atoms are colored pink (carbon), red (oxygen), cyan (nitrogen) and violet (sulfur). Water molecules replaced by the ATP analog are drawn as black spheres in (a), and those conserved in all three structures are drawn as magenta spheres (selected water molecules are numbered). AMPPnP atoms are colored green (carbon), red (oxygen), blue (nitrogen) and orange (phosphorus). In (c), the Mn^{2+} ion and coordinated water molecules are drawn as large and small yellow spheres, respectively. The three sites exhibit a signature feature of all active kinases: the salt bridge between the universally conserved residues Lys 42 and Glu 64. In the ternary complex, the disordered γ -phosphate group is highlighted in white.

site. The overall root mean square (r.m.s.) deviations for 276 C α atoms between Apo-I and either the binary or ternary complexes are both ~ 0.7 Å (Table 2).

Comparison with other kinase catalytic domains

We conducted a comprehensive analysis of the DAPK sequence and three-dimensional structure in the context of other kinase catalytic domains. The five serine/threonine kinases of known X-ray crystal structure, in either an active or inactive conformation, were selected because they share relatively high sequence similarities to DAPK: twitchin kinase²¹, titin kinase²², Ca^{2+} -calmodulin-dependent protein kinase I (CaMKI)²³, phosphorylase kinase (PHK)²⁴ and cyclic AMP-dependent kinase (cAPK)²⁵ (Fig. 3). Most of the discussion of the DAPK catalytic domain structure and active site properties presented here is based on the Apo-I form.

The DAPK catalytic domain and the other kinase catalytic subunits share a number of essential hallmarks, first described for cAPK^{26,27}. DAPK exhibits the familiar bilobal conformation for its smaller, mostly β -stranded N-terminal domain and the larger, helix-rich C-terminal domain (Figs 3, 4a). These two lobes harbor a cleft between them for binding the ATP substrate. The nucleotide-binding fold associates mostly with β -structure, with β -sheets from both domains converging at the active site. Further conserved features include two loops — one located in the small lobe (residues 20–25, DAPK numbering) (Figs 3, 4) and the other in the large lobe (residues 138–144) — and two amino acids triads, one of them harboring Lys 42 (DAPK numbering), which is conserved in protein kinases.

Both in the Apo-I and Apo-II forms, the DAPK catalytic domain adopts a closed, activated conformation. The relative arrangement of domains (Fig. 3) is very similar to the closed conformations established for the cAPK or PHK kinases in complexes with substrates. Movement of the small lobe, associated with the open conformation of the autoinhibited forms of the twitchin, titin and CaMKI kinases, does not affect the conformation of the loop between helix C and the β_4 strand in the N-terminal domain (residues 70–76) (Figs 3, 4a). This loop is part of a short β -sheet that also includes the β_7 and β_8 strands near the hinge region.

Structure determination

The structures of an orthorhombic and a cubic crystal form of the apo DAPK catalytic domain (a 285-residue construct with a 10-residue C-terminal streptavidin-tag) were determined at 1.5 Å (Apo-I, 1 subunit) and 3.5 Å resolution (Apo-II, 2 subunits), respectively. The structure of Apo-I was determined by the single-wavelength anomalous diffraction (SAD) technique based on a single mercury derivative at Cys 30 (Table 1) and represents the highest resolution structure for any protein kinase reported to date. In Apo-I, 276 residues (Tyr 2–Pro 277) of the DAPK catalytic domain are well ordered in the electron density maps (Fig. 2). The fully refined orthorhombic model was then used for structure determination of Apo-II by molecular replacement.

Orthorhombic crystals of the binary complex with AMPPnP were obtained by cocrystallization. Crystals of the ternary complex, consisting of kinase, AMPPnP and either Mg^{2+} or Mn^{2+} , were obtained by soaking the binary complex crystals. Anomalous data collection was performed with Mn^{2+} -containing crystals to verify ion binding sites (Table 1). The structures of ternary complexes in the presence of Mg^{2+} and Mn^{2+} ions were found to be similar, and both feature one bound ion in the active

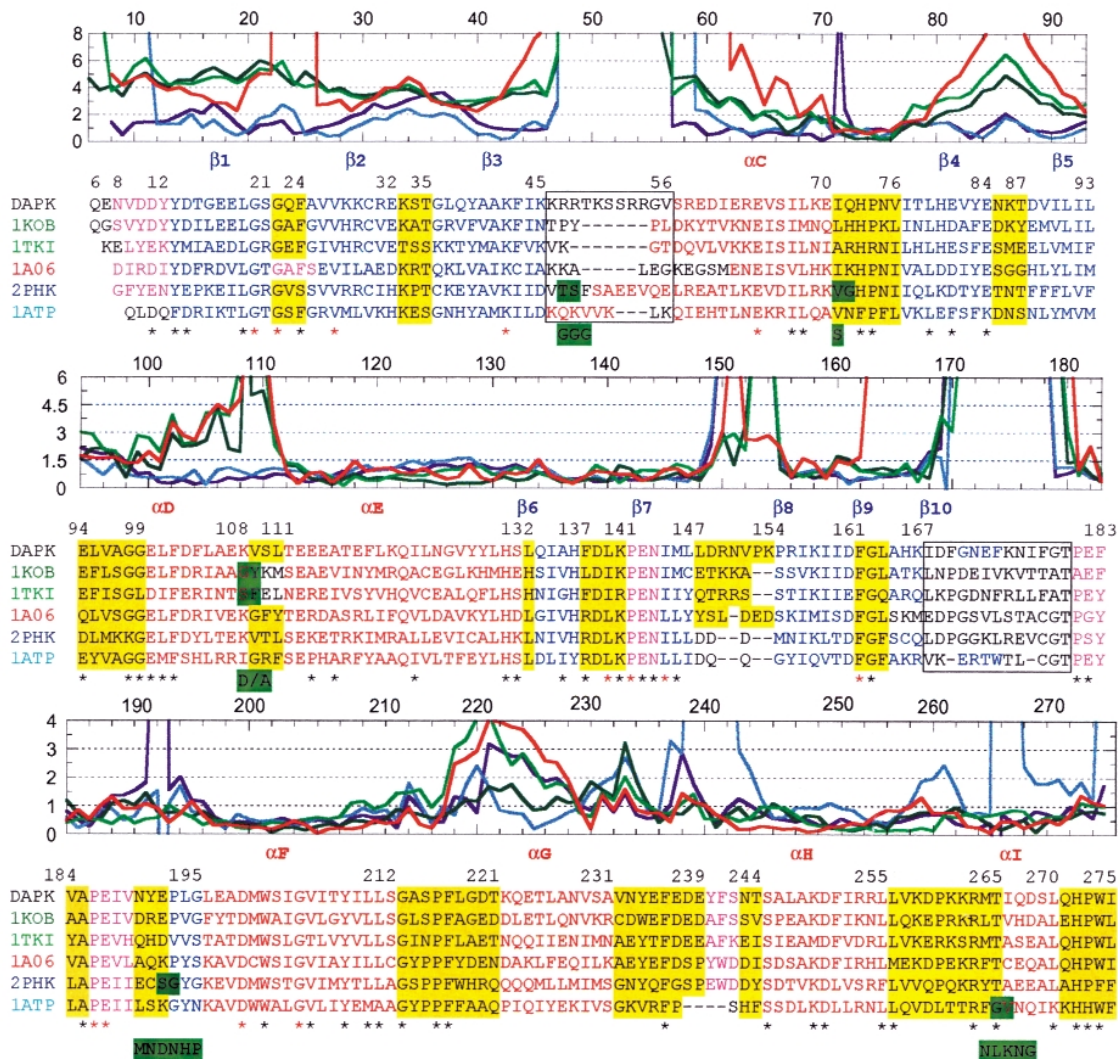


Fig. 3 Structure-based alignment of the DAPK Apo-I structure and five other serine/threonine kinases: twitchin (PDB code 1KOB), titin (1TKI), CaMKI (1A06), PHK (2PHK) and cAPK (1ATP). The graph depicts distances (Å) between corresponding C α atoms of aligned sequences. Vertical lines indicate the loss of correlation between the structure of DAPK and that of the other kinase. The numbering refers to the DAPK catalytic domain. Aligned sequences are colored to match the ribbon diagram of Fig. 4: red for α -helices, blue for β -strands and pink for short α -helical segments. Turns and loops with conserved three-dimensional structure are highlighted in yellow, and those that exhibit loss of correlation with DAPK structure are marked in gray. Residues 46–56 and 168–180 (DAPK numbering) are boxed and constitute unique regions of the DAPK catalytic domain (Fig. 4a). Amino acids conserved in five or six kinases are marked with asterisks. All six sequences contain a number of charged residues that appear universally conserved in the catalytic cores of kinases (red asterisks). Insertions in kinases compared to DAPK are highlighted as green boxes. Deletions in kinases compared to DAPK are dashed lines. The program MOLREP in BLANC³⁸ was used for the alignments.

Packing forces and conformational flexibility

The availability of two crystal forms is helpful for assessing the conformational flexibility of DAPK and for studying the influence of packing forces on its three-dimensional structure. Superposition of the six independent molecules in Apo-I, Apo-II and the AMPPnP-bound complexes reveals several areas of increased conformational variability (Fig. 4c).

The most significant geometric deviations between Apo-I and Apo-II (overall r.m.s. deviation <1.4 Å) occur in the putative peptide binding region preceding helix F of the large lobe and include residues 165–181 and 189–96 (green arrows, Fig. 4c). In addition, the N-terminal region of the G-helix and the loop region immediately before the H-helix in the C-terminal domain exhibit somewhat enhanced conformational freedom (Fig. 4a). Not unexpectedly, the loop between β 7 and β 8, which is part of the interdomain hinge (black arrow), also shows some variation

between the three molecules. However, the N-terminal domain appears to be more rigid by comparison.

The relatively large conformational variations in the peptide binding loop region arise from different packing modes in the orthorhombic and cubic crystals (Fig. 5). Intermolecular interactions in the former include binding a portion of the C-terminal streptavidin-tag between two neighboring kinases (Fig. 5a, only residues Pro 290, Gln 291, Phe 292 and Glu 293 are defined in the electron density maps). When the catalytic domains of the PHK structure with peptide bound and the DAPK structure with tag bound are superimposed, the orientations of peptide and tag differ significantly (not shown). This observation in combination with the fact that the sequences of optimized target peptide and tag are quite different may argue against a functional significance of the mode of binding between tag and activation segment. In Apo-II, two kinase

articles

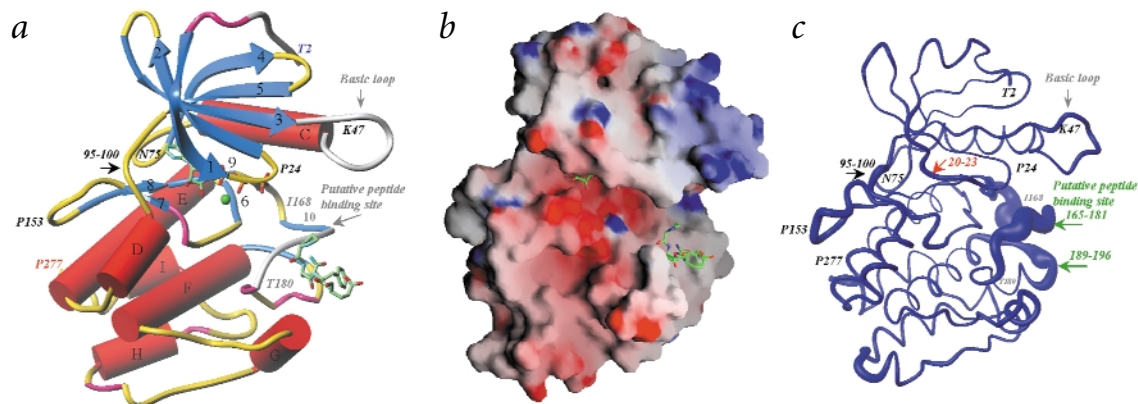


Fig. 4 Overall views of the DAPK catalytic domain. The view is identical in all three panels. **a**, Schematic of the fold. α -helices and β -strands are depicted as red cylinders and blue arrows, respectively; short stretches of α -helical and β -stranded conformation are pink and cyan, respectively; and loop regions are yellow. Residues 46–56 and 168–180 (gray) are unique regions of the DAPK catalytic domain. Selected residues are labeled, and atoms of the bound AMPPnP molecule as well as four residues PQFE from the C-terminal streptavidin-tag of a neighboring molecule bound near the cleft are colored green (carbon), red (oxygen), cyan (nitrogen) and orange (phosphorus). The Mn^{2+} ion coordinated to the α - and β -phosphates is a green sphere. **b**, Electrostatic surface potential calculated with the program GRASP³⁹. Basic and acidic regions appear in blue and red, respectively, with the intensity of the color being proportional to the local potential (energy range -20 to $+12$). The Apo-I structure was used in the calculations. The distributions of the electrostatic potential on the surfaces of kinases differ significantly between individual kinases (not shown). The positively charged crest protruding from the N-terminal lobe of the DAPK catalytic domain represents a unique feature. **c**, Assessment of the conformational flexibility of the DAPK catalytic domain by superimposing the independent protein molecules from the orthorhombic and cubic crystal forms (MOLMOL⁴⁰). The thickness of the line is proportional to the regional deviations between the positions of corresponding α -carbons in individual protein molecules.

molecules face each other pairwise with residues 165–181 and 189–196 (Fig. 5b).

Thus, the interactions between neighboring molecules in the two crystal forms differ considerably (Fig. 5), and lattice forces cannot necessarily account for the preference of the closed and activated states in both of them. Compared to these variations between the Apo-I and Apo-II forms, the conformation of DAPK changes only minimally upon binding of AMPPnP either in the presence or absence of divalent metal ions. Changes include a slight movement (~ 1 Å) of residues 20–23 in the $\beta 1$ strand of the Gly-rich P-loop (red arrows, Fig. 4c).

The ATP binding site

Consistent with the high degree of conservation for several amino acids participating in binding ATP, the active site of the DAPK catalytic domain bears close structural resemblance to those of analyzed serine/threonine kinases. Residues encasing the AMPPnP molecule protrude from the $\beta 1$ – $\beta 2$ – $\beta 3$ sheet, helix C, the loop region linking $\beta 5$ and helix D, as well as the $\beta 6$ – $\beta 7$ region and the $\beta 8$ – $\beta 9$ turn (Figs 2b,c, 6). Although the adenine rings are bound very similarly in the DAPK and cAPK kinases, the comparison between the DAPK and PHK ATP-binding sites reveals minor relative shifts by kinase residues and substrate (Fig. 6a). Amino acids that are conserved and consequently

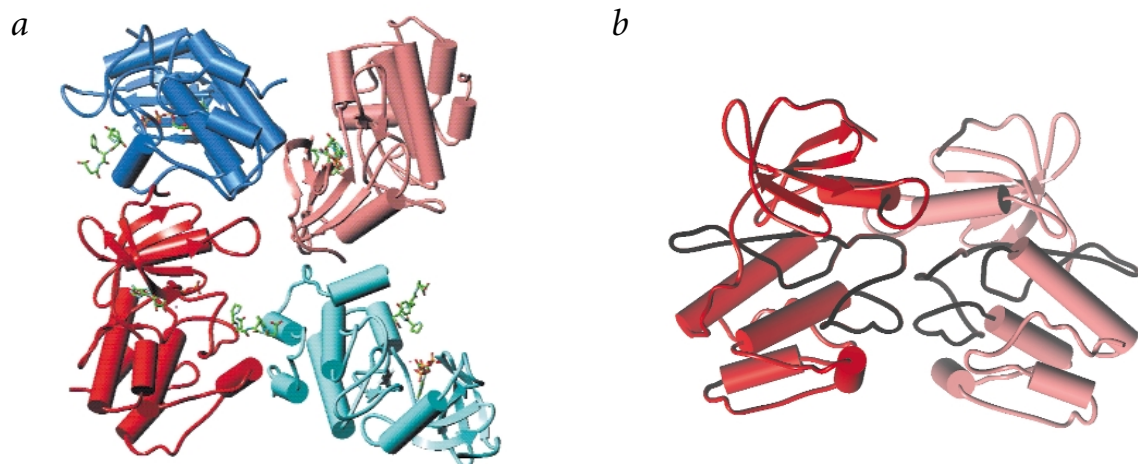
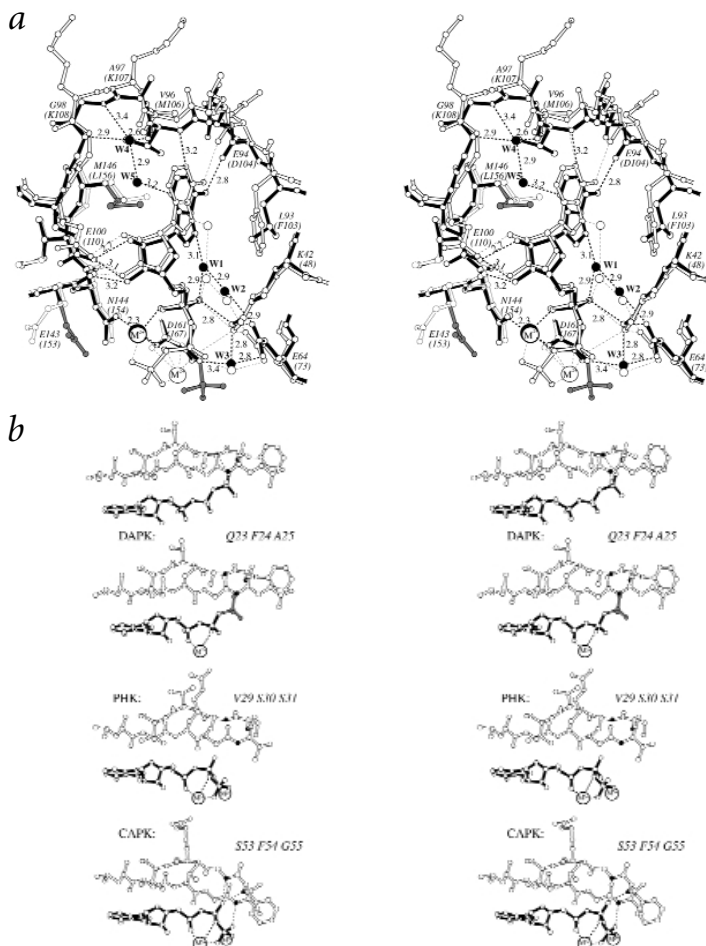


Fig. 5 Lattice interactions in the orthorhombic and cubic crystal forms of the DAPK catalytic domain. **a**, Orthorhombic form. Overview of the environment of the putative peptide-binding region preceding the F-helix and the basic loop linking $\beta 3$ and helix C. Three symmetry mates colored blue, pink and cyan make up the immediate surroundings of the loop region of each DAPK molecule (red). Secondary structure elements are represented as cylinders and arrows, and AMPPnP molecules and four residues of the C-terminal streptavidin-tag visible in the electron density maps are in a ball-and-stick representation. **b**, Cubic form. The crystallographic asymmetric unit consists of DAPK dimers related by a noncrystallographic two-fold rotation axis running approximately along the vertical in the plane of projection. Thus, basic loops and peptide binding regions of the two molecules face each other.

Fig. 6 Active site conformations of kinase-ATP complexes. **a**, Superposition of the active sites of DAPK (orthorhombic form) and phosphorylase kinase (PDB code 2PHK²⁴). The DAPK and PHK substrate complexes are drawn with filled and open bonds, respectively, and amino acids are labeled (numbers in parentheses refer to PHK residues). Ordered water molecules at the active sites of DAPK and PHK are drawn as filled and open circles, respectively, and hydrogen bonds are dashed lines with distances in Å (DAPK). Divalent metal ions are drawn as circles with larger radius: two Mn²⁺ ions (open circles) in the case of PHK and one Mn²⁺ ion (filled circle) in the case of DAPK. The side chains of Glu 143 and Met 146 in DAPK and the γ -phosphate of AMPPnP exhibit multiple conformations and are highlighted in gray. **b**, Conformations of the β 1- β 2 turn and interactions between residues (labeled) of the turn and the nucleotide triphosphate in DAPK, PHK and cAPK. The stereo diagrams depict (from top to bottom): DAPK binary complex (one Mn²⁺ ion), PHK ternary complex (PDB code 2PHK²⁴; two Mn²⁺ ions) and cAPK ternary complex (PDB code 1ATP²⁵; two Mn²⁺ ions). Amino acids of the turn are drawn with open bonds, with selected main chain nitrogen atoms highlighted as filled circles, and bonds of the triphosphate substrates are filled. Hydrogen bonds and metal ion coordinations at the active sites are indicated with thin and thick dashed lines, respectively.



engaged in interactions with virtually identical geometry include Lys 42, Glu 64, Glu 100, Glu 143, Asn 144 and Asp 161 (DAPK numbering, Fig. 6a). Residues Glu 94 and Glu 121 in DAPK and cAPK, respectively, are replaced by Asp 104 in PHK. In all three cases, the carbonyl oxygen is hydrogen bonded to the exocyclic amino group of adenine. Four ordered water molecules are present at all three active sites, but the N7 position of the adenine base is hydrated only in the case of PHK. This water may be engaged in a stacking interaction with Phe 103, a contact that is not possible at the DAPK (Leu 93) or cAPK (Met 120) active sites (Figs 3, 6a).

We located only one metal ion at the ATP binding site of DAPK. Conversely, two Mn²⁺ ions neutralize the negative charges of phosphates in the PHK and cAPK kinase-substrate complexes (Fig. 6). In the binary AMPPnP complex of DAPK, the γ -phosphate group is directed toward the Gly-rich loop and forms a hydrogen bond to three amide groups of the β 1- β 2 turn (Fig. 6b). In the ternary complex, with one Mn²⁺ or Mg²⁺ ion bridging the α - and β -phosphates, the γ -phosphate is disordered, and the β -phosphate is slightly rotated from its position in the binary complex. In the PHK-substrate and cAPK-substrate complexes with two bound ions, the second ion bridges the β - and γ -phosphates, thus stabilizing the conformation of the γ -phosphate. In the PHK-substrate complex, there are no hydrogen bonding interactions between phosphate oxygens and main or side chain kinase atoms (Fig. 6b). By comparison, at the active site of the cAPK-substrate complex, the β -phosphate group is engaged in hydrogen bonds to amide groups from the Gly-rich loop, which is inclined toward the phosphate moiety in this case.

Solvent structure at the active site

The high resolution structures of the DAPK apo form, as well as the kinase-AMPPnP complexes in the absence and presence of a divalent metal ion, allow an analysis of the movements of active site residues upon binding of substrate and the ensuing changes in the water structure. From the stereo diagrams (Fig. 2), significant changes in the main chain conformations of active site residues are necessary to accommodate the substrate. Of the total of 26 ordered waters observed at the ATP binding site in Apo-I (Fig. 2a), 14 occupy virtually identical positions in the

binary (Fig. 2b) and ternary complexes (Fig. 2c). The ammonium group of the universally conserved Lys (residue 42 in DAPK) is surrounded by eight oxygen atoms, contributed by the α - and β -phosphate groups, Glu 64 and three water molecules (Figs 2, 6a). This previously undescribed mode of interaction is reminiscent of the complexation of alkali metal ions and ammonium ions by crown ethers²⁸. At the DAPK active site with one ion bound, only one nonbridging α -phosphate oxygen forms a hydrogen bond with Lys 42. In the PHK and cAPK structures with two ions bound at the active sites, both α - and β -phosphate oxygens form hydrogen bonds to this conserved Lys residue.

DAPK 'fingerprint' regions

A DAPK region of apparently unique sequence and three-dimensional structure emerges from the alignments (Fig. 3) and electrostatic surface potential calculations (Fig. 4b). This region concerns a stretch of mostly basic residues, starting with Lys 45 and ending with Val 56. It connects β 3 and helix C and maps to the surface of the N-terminal domain, effectively protruding from it and constituting a 'lid' above the putative peptide binding ledge (Fig. 4a, gray loops on the right). The loop contains no less than seven Arg and Lys residues, including Lys 45 at the C-terminal end of β 3. Further contributions to the positive potential of this area stem from Lys 86 located in the short loop between β 4 and β 5 (Figs 3, 4a) as well as Arg 58 near the N-terminal end of the C-helix. This portion of DAPK is characterized by a complete lack of correlation in the three-dimensional structural alignments (Fig. 3). The detailed con-

articles

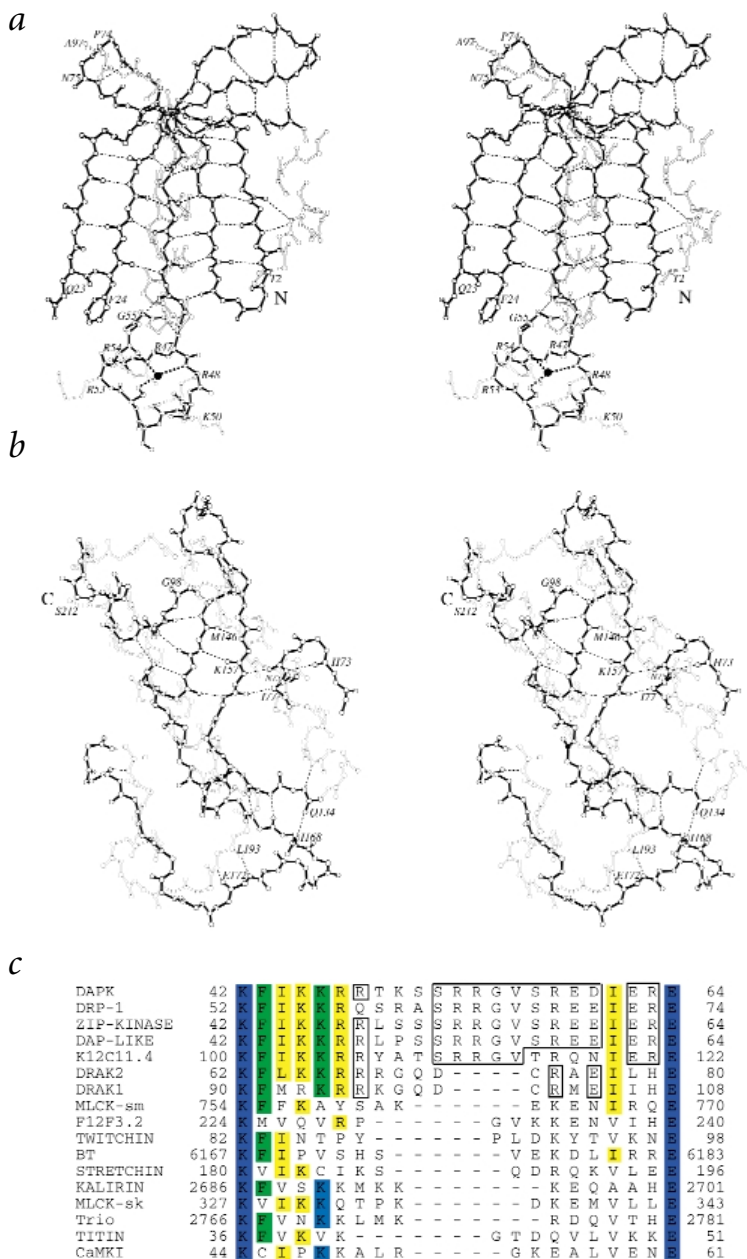




Table 1 SAD data collection

Crystal data	Hg-SAD	Mn-SAD
Space Group	P2 ₁ 2 ₁ 2 ₁	P2 ₁ 2 ₁ 2 ₁
Unit cell parameters (Å)		
a	46.92	46.58
b	62.55	62.19
c	88.56	88.51
X-ray source	DND-CAT: 5ID	IMCA-CAT: 17ID
Wavelength (Å)	1.00928	1.89200
Resolution (Å)		
Range	20–1.8	20–2.5
Last shell	1.86–1.80	2.59–2.50
Unique reflections ¹	24,944 (2,451)	9,277 (910)
Redundancy	6.5	5.9
Completeness ¹ (%)	99.9 (99.7)	99.8 (99.1)
R _{merge} ^{1,2}	0.041 (0.278)	0.071 (0.178)
SAD statistics		
ΔF ³	0.58	0.50
Phasing power	1.28	–
Figure of merit ⁴	0.29 / 0.87	–

¹Values in parentheses correspond to the last resolution shell.

²R_{merge} = $\sum_{hkl} \sum_i |I(hkl)_i - \langle I(hkl) \rangle| / \sum_{hkl} \sum_i \langle I(hkl) \rangle$ over *i* observations of a reflection *hkl*.

³ΔF = $(\langle |F(+)| \rangle - |F(-)|)^2 / (1/2(\langle |F(+)| \rangle^2 + \langle |F(-)| \rangle^2))^{1/2}$.

⁴Prior and after density modification.

potential functional role this unique basic loop structure plays in enzyme function.

Although the answer to this question must await additional studies, the structure suggests priorities for future research. For example, several of the basic loop residues are conserved among the members of the death-associated protein kinase family¹⁵. They include Lys 46, Arg 47, Arg 48 (DAPK numbering; exception Gln 48 in DRP-1), Arg 53 (Lys 53 in DRAK-1), Arg 54 (Gly 54 in DRAK-1 and DRAK-2) and Arg 58 (Fig. 7c). The presence of the loop structure in death kinases, some of which are not CaM regulated enzymes, argues against the involvement of the novel basic loop structure of DAPK in a classical CaM-regulated kinase autoinhibition²⁹. Autoinhibitory domains in CaM-regulated kinases are usually located farther downstream in the amino acid sequence, on the carboxyl terminal end of the catalytic domain, and usually feature clusters of basic residues. Further, DAPK has a potential autoinhibitory domain based on its high sequence similarity to MLCK, and this potential autoinhibitory sequence segment is not included within the catalytic domain sequence.

Therefore, several arguments suggest that the unique loop structure of DAPK is not involved in CaM regulation of the enzyme. In contrast, the conservation of the corresponding amino acid sequence across death kinases raises the possibility that this loop might be associated with the regulation of death kinases. One common feature among death kinases is the critical need for a cell to keep the enzyme activity turned off until needed for programmed cell death. The location of the loop in the DAPK catalytic structure near the peptide recognition region raises the possibility that this could be a site of interaction with a regulatory protein or a site of modification in DAPK that would regulate its kinase activity. Clearly, much remains to be determined, but the availability of the DAPK catalytic domain structure has revealed logical next steps in attempts to understand the mechanism of action and regulation of death kinases.

Conclusions

In addition to conformational features common to all catalytic domains of protein kinases, the crystal structure of the DAPK catalytic domain at high resolution has revealed an unusual highly basic, structured loop in the N-terminal domain (Figs 3, 4). The loop extends from the mouth of the ATP-binding cleft that lies between the two domains. Thus, it is situated above a portion of the putative peptide-binding ledge, creating a positively charged patch on the molecular surface of DAPK (Fig. 4b). Because the physiological targets of DAPK have not been defined to date, assigning a definitive function to this loop is not yet possible. However, the observation that the basic loop structure is conserved across death kinases but not found in other kinases argues for a functional importance. The charge properties of the loop and its presence in death kinases that are not CaM regulated argue against its involvement in CaM-regulated autoinhibition. Given their role in apoptosis, the catalytic domain of death kinases may likely be kept in check by additional regulatory mechanisms; the loop region may be involved in such critical regulation. Thus, our structures provide new insights into the potential regulation and functioning of the family of death-associated protein kinases. Our work should benefit the structure-assisted discovery of new active site-directed inhibitors of DAPK that may serve as key research reagents to dissect the role of DAPK in cellular function. Also, our results lay a firm foundation for future investigations into the potential of DAPK being a target for therapeutics in the treatment of a range of neurodegenerative diseases.

Methods

Protein overexpression and purification. A DAPK construct, comprising amino acids Met 1–Ser 285 and a C-terminal streptavidin-tag (286-SAWSHQPFEK-295), was subcloned into the pASK-IBA3 (Genosys Biotechnologies Inc.) expression vector at the *Bsal* sites. The protein was produced and purified from *E. coli* essentially as described³⁰.

Crystallization. Crystallization conditions were determined with sparse-matrix screens (Hampton Research and Emerald Biostructures Inc.) using the hanging drop vapor diffusion technique. For the orthorhombic crystal form (Apo-I), aqueous protein solution (6 mg ml⁻¹) in 20 mM Tris-HCl, pH 7.5, 1 mM dithiothreitol (DTT), 1 mM EDTA and 0.1 M NaCl was mixed with an equal volume of reservoir buffer, containing 1.6 M ammonium sulfate, pH 8.0 (or 1.5 M Li sulfate, pH 7.5). Droplets were equilibrated against 0.5 ml reservoirs. The mercury derivative was obtained by soaking orthorhombic DAPK crystals in crystallization buffer supplemented with 0.5 mM CH₃HgCl for two days. For the cubic crystal form (Apo-II), equal volumes of the above protein solution and a solution containing 5% (w/v) PEG-1000, 40% (v/v) PEG-300 and 0.1 M Tris-HCl, pH 7.0, were mixed, and droplets were equilibrated against 0.5 ml reservoirs. For the DAPK–nucleotide complexes, orthorhombic crystals were grown by mixing equal volumes of protein solution, preincubated with 2 mM AMPpP for 30 min, with reservoir solution (1.6 M ammonium sulfate and 100 mM Tris-HCl, pH 8.0), and equilibrating the droplets against 0.5 ml reservoirs. Crystals were soaked in reservoir solution supplemented with 50 mM metal ions (MnSO₄ or MgCl₂).

Data collection and processing. Apo-I crystals were shock-frozen in mother liquor supplemented with 25% (v/v) glycerol. Diffraction data were collected at 100 K on the 5-ID beam line of the DND-CAT at the Advanced Photon Source (APS), Argonne, Illinois. SAD data were collected at 1.00928 Å using a single Hg-DAPK crystal. All data were integrated and merged in the DENZO/SCALEPACK program suite³¹. Details regarding anomalous data collection are listed in Table 1, and selected crystal data and diffraction data statistics for native crystals are summarized in Table 2. To maximize the anomalous contribution of Mn²⁺, data were collected at 1.8923 Å (17-ID



articles

Table 2 Crystal data, data collection and refinement statistics

	Apo-I	AMPPnP	AMPPnP-Mn ²⁺	AMPPnP-Mg ²⁺	Apo-II
Crystal data					
Crystal system		orthorhombic			tetragonal
Space group	P2 ₁ 2 ₁ 2 ₁	P4 ₁			
Unit cell parameters (Å)					
a	46.93	46.74	46.71	46.63	58.37
b	62.55	62.4	62.34	62.43	58.37
c	88.56	88.11	88.6	88.67	212.61
Asymmetric unit (residues)					
Protein / AMPPnP	280 / 0	280 / 1	280 / 1	280 / 1	2 × 276 / –
Water / ion	353 / –	247 / –	267 / 1 Mn ²⁺	132 / 1 Mg ²⁺	–
Data collection					
X-ray source	DND-5ID	DND-5ID	IMCA-17ID	IMCA-17ID	DND-ID
Wavelength (Å)	1.00928	1.2562	0.979	0.984	1.000
Resolution (Å)					
Range	20–1.50	20–1.62	20–1.80	20–2.40	20–3.50
Last shell	1.55–1.50	1.68–1.62	1.86–1.80	2.49–2.40	4.0–3.50
Unique reflections ¹	41,549 (3,938)	32,120 (2,936)	24,665 (2,294)	10,555 (1,033)	8,704 (892)
Redundancy	5.4	6.0	6.9	4.5	5.4
Completeness ¹ (%)	97.7 (94.2)	97.7 (94.2)	99.9 (99.8)	99.8 (99.9)	96.5 (96.1)
R _{merge} ^{1,2}	0.037 (0.27)	0.037 (0.27)	0.061 (0.36)	0.070 (0.30)	0.072 (0.39)
Refinement (F > 0)					
Reflections					
Work	36,218	27,906	21,099	8,877	7,597
Free	4,044	3,096	2,341	1,011	903
R-factor	0.183	0.201	0.189	0.201	0.272
R _{free}	0.202	0.218	0.214	0.239	0.297
R.m.s. deviation					
Bond lengths (Å)	0.005	0.010	0.011	0.007	0.009
Bond angles (°)	1.22	1.25	1.29	1.29	1.69
Average B- factors (Å ²)					
Protein / AMPPnP	19.2 / –	19.9 / 35.8	22.1 / 20.5	27.6 / 37.9	45.5 / –
Water / ion	32.2 / –	30.3 / –	36.2 / 23.3	36.9 / 69.3	–

¹Values in parentheses correspond to the last resolution shell. All data (F > 0) were used in the refinement.

²R_{merge} = $\sum_{hkl} \sum_i |I(hkl)_i - \langle I(hkl) \rangle| / \sum_{hkl} \sum_i \langle I(hkl) \rangle$ over *i* observations of a reflection *hkl*.

beam line, IMCA-CAT, APS). An Apo-II crystal was shock-frozen in mother liquor, and diffraction data were collected on the 5-ID beamline of the DND-CAT at the APS (Table 2).

Structure determination and refinement. Phases for the Apo-I crystal form were initially determined with the SAD technique using CNS³². Solvent flipping was applied and significantly improved the initial electron density maps. Automatic model building was performed with WARP³³. The resulting model was completed manually using TURBO-FRODO³⁴. The structures of the binary and ternary complexes, as well as the Apo-II form, were determined by the molecular replacement with AMoRe³⁵. Positional, simulated annealing and temperature factor refinements were performed using CNS³². R_{free} was monitored by setting aside 10% of the reflection as a test set (Table 2)³⁶. The Ramachandran plot calculated with PROCHECK³⁷ indicates that 100% of the non-Gly and non-Pro residues in the final models lie in the most favored and additional allowed regions.

Coordinates. Coordinates and structure factors for all described structures have been deposited in the Protein Data Bank (1JKS

(Apo-I), 1JKL (binary), 1IG1 (ternary, Mn), 1JJK (ternary, Mg) and 1JKT (Apo-II)).

Acknowledgments

This work was supported in part by a NIH grant to M.E. and in part by grants from the Alzheimer's Association, the Institute for the Study of Aging and the NIH to D.M.W. We are grateful to W.F. Anderson, T.J. Lukas, G. Minasov and A. Velentza for expert assistance during the various stages of the project. Use of the Advanced Photon Source was supported by the U.S. Department of Energy, Basic Energy Sciences, Office of Science. The DuPont-Northwestern-Dow Collaborative Access Team (DND-CAT) Synchrotron Research Center at the Advanced Photon Source (Sector 5) is supported by E. I. DuPont de Nemours & Co., The Dow Chemical Company, the National Science Foundation and the State of Illinois. The Industrial Macromolecular Crystallography Association Collaborative Access Team (IMCA-CAT) at the Advanced Photon Source (Sector 17) is supported by the companies of the Industrial Macromolecular Crystallography Association through a contract with the Illinois Institute of Technology (IIT), executed through the IIT's Center for Synchrotron Radiation Research and Instrumentation.

Received 30 April, 2001; accepted 27 August, 2001.



1. Laster, S.M., Wood, J.G. & Gooding, L.R. Tumor necrosis factor can induce both apoptotic and necrotic forms of cell lysis. *J. Immunol.* **141**, 2629–2634 (1988).
2. Trauth, B.C. *et al.* Monoclonal antibody-mediated tumor regression by induction of apoptosis. *Science* **245**, 301–305 (1989).
3. Itoh, N. *et al.* The polypeptide encoded by the cDNA for human cell surface antigen Fas can mediate apoptosis. *Cell* **66**, 233–243 (1991).
4. Lin, J.K. & Chou, C.K. *In vitro* apoptosis in the human hepatoma cell line induced by transforming growth factor β 1. *Cancer Res.* **52**, 385–388 (1992).
5. Novelli, F. *et al.* Environmental signals influencing expression of the IFN- γ receptor on human T cells control whether IFN- γ promotes proliferation of apoptosis. *J. Immunol.* **152**, 496–504 (1994).
6. Gjertsen, B. & Doskeland, S. Protein phosphorylation in apoptosis. *Biochim. Biophys. Acta* **1269**, 187–189 (1995).
7. Anderson, P. Kinase cascades regulating entry into apoptosis. *Microbiol. Molec. Biol. Rev.* **61**, 33–46 (1997).
8. Inbal, B. *et al.* DAP kinase links the control of apoptosis to metastasis. *Nature* **390**, 180–184 (1997).
9. Raveh, T., Droguett, G., Horvitz, M.S., DePinho, R.A. & Kimchi, A. DAP kinase activates a p19^{ARF}/p53-mediated apoptotic checkpoint to suppress oncogenic transformation. *Nature Cell Biol.* **3**, 1–7 (2001).
10. Cohen, O., Feinstein, E. & Kimchi, A. DAP-kinase is a Ca²⁺/calmodulin-dependent kinase, with cell death-inducing functions that depend on its catalytic activity. *EMBO J.* **16**, 998–1008 (1997).
11. Kimchi, A. DAP genes: novel apoptotic genes isolated by a functional approach to gene cloning. *Biochim. Biophys. Acta* **1377**, 13–33 (1998).
12. Cohen, O. *et al.* DAP-kinase participates in TNF α - and Fas-induced apoptosis and its function requires the death domain. *J. Cell. Biol.* **146**, 141–148 (1999).
13. Raveh, T., Berissi, H., Eisenstein, M., Spivak, T. & Kimchi, A. A functional genetic screen identifies regions at the C-terminal tail and death-domain of death-associated protein kinase that are critical for its proapoptotic activity. *Proc. Natl. Acad. Sci. USA* **97**, 1572–1577 (2000).
14. Kawai, T. *et al.* Death-associated protein kinase 2 is a new calcium/calmodulin-dependent protein kinase that signals apoptosis through its catalytic activity. *Oncogene* **18**, 3471–3480 (1999).
15. Inbal, B., Shani, G., Cohen, O., Kissil, J.L. & Kimchi, A. Death-associated protein kinase-related protein 1, a novel serine/threonine kinase involved in apoptosis. *Mol. Cell Biol.* **18**, 1642–1651 (2000).
16. Kawai, T., Matusmoto, M., Takeda, K., Sanjo, H. & Akira, S. ZIP-kinase, a novel serine/threonine kinase which mediates apoptosis. *Mol. Cell Biol.* **18**, 1642–1651 (1998).
17. Kogel, D., Plottner, O., Landsberg, G., Christian, S. & Scheidtmann, K.H. Cloning and characterization of Dlk, a novel serine/threonine kinase that is tightly associated with chromatin and phosphorylates core histones. *Oncogene* **17**, 2645–2654 (1998).
18. Sanjo, H., Kawai, T. & Akira, S. DRAKs, novel serine/threonine kinases related to death-associated protein kinase that trigger apoptosis. *J. Biol. Chem.* **273**, 29066–29071 (1998).
19. Shani, G. *et al.* Autophosphorylation restrains the apoptotic activity of DRP-1 kinase by controlling dimerization and calmodulin binding. *EMBO J.* **20**, 1099–1113 (2001).
20. Velentza, A.V., Schumacher, A.M., Weiss, C., Egli, M. & Watterson, D.M. A protein kinase associated with apoptosis and tumor suppression: structure, activity and discovery of peptide substrates. *J. Biol. Chem.* **In the press** (2001).
21. Kobe, B. *et al.* Giant protein kinases: domain interactions and structural basis for autoregulation. *EMBO J.* **15**, 6810–6821 (1996).
22. Mayans, O. *et al.* Structural basis for activation of the titin kinase domain during myofibrillogenesis. *Nature* **395**, 863–868 (1998).
23. Goldberg, J., Nairn, A.C. & Kuriyan, J. Structural basis for the autoinhibition of calcium/calmodulin-dependent protein kinase I. *Cell* **84**, 875–887 (1996).
24. Lowe, E.D. *et al.* The crystal structure of a phosphorylase kinase peptide substrate complex: kinase substrate recognition. *EMBO J.* **16**, 6646–6658 (1997).
25. Zheng, J. *et al.* 2.2 Å refined crystal structure of the catalytic subunit of cAMP-dependent protein kinase complexed with MNATP and a peptide inhibitor. *Acta Crystallogr. D* **49**, 362–365 (1993).
26. Knighton, D.R. *et al.* Crystal structure of the catalytic subunit of cyclic adenosine monophosphate-dependent protein kinase. *Science* **253**, 407–414 (1991).
27. Knighton, D.R. *et al.* Structure of a peptide inhibitor bound to the catalytic subunit of cyclic adenosine monophosphate-dependent protein kinase. *Science* **253**, 414–420 (1991).
28. Dobler, M. *Ionophores and their structures* (Wiley, New York; 1981).
29. Lukas, T.J., Mirzoeva, S. & Watterson, D.M. In *Calmodulin and signal transduction* (eds. Van Eldik, L. & Watterson, D.M.) 65–168 (Academic Press, San Diego; 1998).
30. Shoemaker, M. O. *et al.* Use of DNA sequence and mutant analyses and antisense oligodeoxynucleotides to examine the molecular basis of nonmuscle myosin light chain kinase autoinhibition, calmodulin recognition, and activity. *J. Cell. Biol.* **111**, 1107–1125 (1990).
31. Otwinowski, Z. & Minor, W. Processing of X-ray diffraction data collected in oscillation mode. *Methods Enzymol.* **276**, 307–326 (1997).
32. Brünger, A.T. *Crystallography & NMR system (CNS), Version 0.9* (Yale University, New Haven; 1998).
33. Perrakis, A., Morris, R. & Lamzin, V.S. Automated protein model building combined with iterative structure refinement. *Nature Struct. Biol.* **6**, 458–463 (1999).
34. Cambillau, C. & Roussel, A. *Turbo Frodo, Version OpenGL.1* (Université Aix-Marseille II, Marseille; 1997).
35. Navaza, J. AMoRe: an automated package for molecular replacement. *Acta Crystallogr. A* **50**, 157–163 (1994).
36. Brünger, A.T. Free R value: a novel statistical quantity for assessing the accuracy of crystal structures. *Nature* **355**, 472–475 (1992).
37. Collaborative Computational Project, Number 4. The CCP4 suite: programs for protein crystallography. *Acta Crystallogr. D* **50**, 760–763 (1994).
38. Vagin, A. A., Murshudov, G. N. & Stropkopytov, B. V. BLANC: the program suite for protein crystallography. *J. Appl. Crystallogr.* **31**, 98–102 (1998).
39. Nicholls, A., Sharp, K.A. & Honig, B. Protein folding and association: insights from the interfacial and thermodynamic properties of hydrocarbons. *Protein Struct. Func. Genet.* **11**, 281–296 (1991).
40. Koradi, R., Billeter, M. & Wüthrich, K. MOLMOL, a program for display and analysis of macromolecular structures. *J. Mol. Graphics* **14**, 51–55 (1996).